ELSEVIER

International Journal of Mass Spectrometry 206 (2001) 137–151

International Journal of Mass Spectrometry

Current–voltage characteristics in a flame plasma: analysis for positive and negative ions, with applications

John M. Goodings[a,*], Jingzhong Guo[a], Allan N. Hayhurst[b], Stephen G. Taylor[b]

[a]*Department of Chemistry and Centre for Research in Mass Spectrometry, York University, 4700 Keele Street, Toronto, Ontario M3J 1P3, Canada*

[b]*Department of Chemical Engineering, University of Cambridge, Pembroke Street, Cambridge, CB2 3RA, England*

Received 3 July 2000; accepted 30 October 2000

Abstract

A flat, cylindrical, laminar, H_2–O_2–N_2 flame in plug flow with velocity $v_f = 19.8$ m s^{-1} and cross-sectional area $A = 1.05 \times 10^{-4}$ m^2, at 1 atm and 2400 K, was doped with appropriate additives to give a weak, continuum, quasi-neutral plasma involving Cs^+/e^- or H_3O^+/e^- or $H_3O^+/Cl^-/e^-$. The flame impinged on a planar, normal, water-cooled, conducting electrode designated N (for nozzle) located a variable distance z downstream from the flame's luminous reaction zone which is separated by a dark space or gap $\delta \simeq 1$ mm from a water-cooled metallic burner B, the second electrode. Neither electrode has the properties of a Langmuir probe. Two types of data were measured: i–V characteristics with the current i(N) collected by the nozzle versus the applied voltage $\Delta\varphi$ between N and B at a fixed value of z (e.g. 20 mm); and profiles of i(N) versus z at a fixed value of $\Delta\varphi$. For $\Delta\varphi < 0$ (e.g. -50 V; N is negative), the electrons are stopped in the flame and the constant saturation current is controlled by the convective flow of positive ions to the nozzle: $i_+(\mathrm{N}) = eAn_+(\mathrm{N})v_f$. This provides a wonderfully simple and accurate measurement of the absolute density n_+(N). Alternatively, if a weak solution of a Cs salt (e.g. 10^{-4} M CsCl) is sprayed using a pneumatic atomizer such that Cs is completely ionized, the delivery factor of the atomizer can be calibrated. Furthermore, if the delivery factor giving n_+(N) is known, v_f can be determined. With $\Delta\varphi$ fixed (e.g. -50 V), a profile of n_+(N) versus z can be obtained throughout the flame gas downstream; the density distribution is not affected by the application of the applied voltage. For $\Delta\varphi > 0$ (e.g. $+50$ V, N is positive), the current through the flame $i_+(\mathrm{B}) = -i_e(\mathrm{N}) - i_-(\mathrm{N})$ (the latter term is included if negative ions are present), is controlled by the flow of positive ions of mobility μ_+ to the burner across the potential gradient in the burner gap g: $i_+(\mathrm{B}) = eAn_+(\mathrm{B})\mu_+\nabla\varphi_g$. When $\Delta\varphi$ is sufficiently positive to achieve a constant saturation current, n_+(B) can be determined; it represents the total ion production in the flame reaction zone. When negative ions are present replacing even a large fraction of the electrons, the effect on the i–V characteristic is relatively minor; it does not appear possible to provide a separate analysis for n_e and n_-. However, profiles through the flame plasma clearly show the effects of negative ion processes such as ion–ion recombination, for example. For a wide range of the applied voltage $\Delta\varphi$, both positive and negative, it is possible to calculate the potential distribution in the burner gap, the bulk flame plasma and in the positive ion sheath at the nozzle. This provides a quantitative understanding of the ion and electron behaviour throughout the flame. (Int J Mass Spectrom 206 (2001) 137–151) © 2001 Elsevier Science B.V.

Keywords: Flame ionization; Flame plasma; Current–voltage characteristics; Negative ions

* Corresponding author. E-mail: goodings@yorku.ca

1387-3806/01/$20.00 © 2001 Elsevier Science B.V. All rights reserved
PII S1387-3806(00)00398-5

1. Introduction

Ions in a flame at 1 atm pressure can be sampled through a nozzle into a mass spectrometer at a much lower pressure. Sampling perturbations can result primarily from two causes. The first is the inevitable cooling which occurs when the sample passes through the nozzle [1,2]. The second perturbation, with which this article is concerned, stems from the fact that the flame is a weak, flowing, continuum plasma which forms a plasma sheath or potential gradient at both the metallic nozzle and burner. Thus, it is not surprising that the sampling conditions vary when a voltage is applied between the nozzle and the burner. The phenomenon was first considered when measuring ion concentrations in a flame [3]. The effect of applied electric fields on the mass-spectrometric sampling of both positive and negative ions was investigated further when using a needle to collect charged particles inside the conical sampling nozzle, just behind the orifice in the nozzle tip [4–6].

When the voltage applied between the nozzle and burner is varied, the sampling nozzle and its water-cooled mounting plate collect a net current, either positive or negative; the burner must receive an equal current of opposite sign. We first measured these current–voltage characteristics to explain a discrepancy in the sampled ion current when a large multi-tube burner was employed instead of a small single-tube burner [7]. Essential background for an understanding of the characteristics is provided by recent work on probe theory for a high-pressure plasma, including experimental work using a flame at atmospheric pressure [8,9]. These studies, which concentrate on the electron current to a positively biased probe [10], follow the pioneering work of Su and Lam [11,12], primarily concerned with the collection of positive ions on a negatively biased probe in a flowing continuum plasma.

Our original, and still primary, objective for undertaking this study was to inquire into the integrity of sampling flame ions through a nozzle orifice into a mass spectrometer when a voltage is applied between the nozzle plate and the burner. There is inevitably an electric field at the sampling nozzle, so the application of an applied voltage is an obvious thing to do. It does not follow, a priori, that the application of zero voltage (both electrodes, say, at earth potential) achieves "correct" sampling. Under most conditions, the nozzle is covered by an electrical sheath from which the ion sample is extracted. It is unlikely that the effect of this sheath on the sampling of positive and negative ions would be the same. Therefore, it is necessary to understand what happens to the ions, both positive and negative, when the flame plasma flows onto the nozzle electrode.

Considerable insight into these matters can be gleaned from a detailed understanding of the current–voltage (i–V) characteristics measured between the burner and the nozzle plate. Also, it became apparent in this study that the i–V characteristics provide valuable information in addition to their utility for sampling diagnostics: one important application is the measurement of absolute ion densities in the flame plasma. Further, it will be seen that a i–V characteristic can enable the velocity of the flame gas downstream to be determined. Alternatively, the delivery of the pneumatic atomizer used to nebulize aqueous solutions of a metallic salt into the gas supplies to a flame can be calibrated. A different part of the characteristic yields the total ion production rate. This study deals with a simple flame containing trace quantities of free electrons e^-, the positive ions Cs^+ or H_3O^+ and the negative Cl^- ion.

2. Experimental

The very simple apparatus employed at both York and Cambridge Universities for these studies is shown in Fig. 1. The metallic sampling nozzle mounted in a water-cooled stainless steel sampling plate is bolted to the front flange of the mass spectrometer [13]. The front flange, sampling plate, and nozzle are connected together and electrically isolated from earth; henceforth, the term "nozzle" will be used to refer to such a collective assembly as one single electrode, designated by N. Equally well, a simple flat plate (probably water-cooled) or mesh grid could be employed. The nozzle potential with respect to earth could be varied

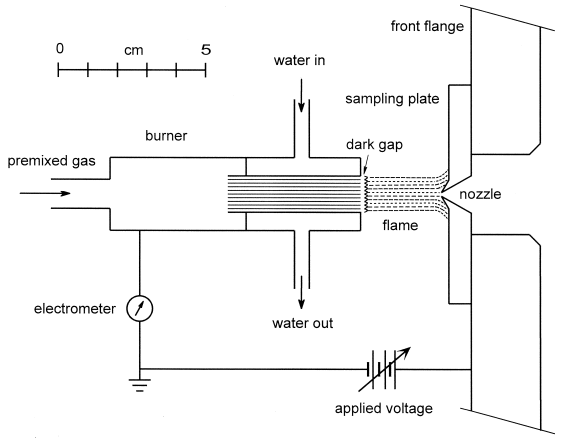

Fig. 1. Schematic diagram of the apparatus employed to measure current–voltage characteristics and axial concentration profiles of a flame plasma.

Table 1
Properties of the hydrogen–oxygen–nitrogen flame

Property	Value
Equivalence ratio Φ	1.37
$H_2/O_2/N_2$	2.74/1/2.95
Total unburnt gas flow $\dot{V}$	300 $cm^3\ s^{-1}$
Measured flame temperature T_f	2400 K
Velocity in the burnt gas v_f	19.8 $m\ s^{-1}$
Flame diameter d	11.6 mm
Cross-sectional area A	$1.05 \times 10^{-4}\ m^2$
Mole ratio r, unburnt/burnt gas	1.1695
Equilibrium burnt gas composition	Mole fraction
H_2O	0.3460
H_2	0.1286
O_2	0.0001057
H	0.006019
OH	0.003084
O	0.00009469
N_2	0.5157

in the range from −100 to +100 V. The metallic burner which constitutes the second electrode, designated B, was also electrically isolated on ceramic supports and connected to earth through an electrometer (Keithley, model 616). The flat-flame burner itself [13] consisted of 151 stainless steel hypodermic tubes in a close-packed circular array mounted in a water-cooled brass body. To achieve good electrical isolation, cooling water for the burner was supplied by gravity from an elevated and isolated water tank and appropriate plastic tubing. Obviously, other types of metallic burners could be employed.

For the measurement of profiles of current (to the nozzle or burner) versus distance z (0–30 mm) along the flame axis (at fixed applied voltage), the burner was mounted on a motor-driven carriage with digital read-out of the axial distance. The designation of $z = 0$ is taken as the point where the nozzle pokes through the bright luminous flame reaction zone into the cold unburnt gas upstream, giving an abrupt pressure rise on an ionization gauge located in the vacuum chamber of the mass spectrometer [13]. This method is more accurate when results from different flames are to be compared. However, the distance between the burner and the nozzle electrode could be used as a measure of the axial distance z. Both the i–V characteristics and the profiles were recorded on an XY plotter with current i on the Y axis versus either the applied voltage $\Delta\varphi$ or z on the X axis, respectively.

The sign convention for the applied potential difference is given by $\Delta\varphi = \varphi_{\text{nozzle}} - \varphi_{\text{burner}}$; a positive $\Delta\varphi$ means that the nozzle is positive with respect to the burner. In terms of the applied voltage, $\Delta\varphi = V_{\text{nozzle}}$ because the resistance through the electrometer to earth is negligible. Since the flame is a quasi-neutral plasma, a net current collected by the nozzle will be matched by an equal current of opposite sign collected by the burner. Consistent with the sign convention employed for $\Delta\varphi$, the sign of any current i in the figures below is referenced to the nozzle; i.e. a positive i means that the electrode N is collecting a positive current (with an equal negative current to the burner) and vice versa. In practice, it was easier to achieve electrical isolation of the burner and to measure its current rather than the current to the nozzle.

The H_2–O_2–N_2 flame employed for these studies has been well-characterized previously (designated "flame 2"); its properties are given in Table 1. It is a premixed laminar flame of fuel-rich composition burning at atmospheric pressure with the cylindrical burnt gas (diameter 11.6 mm) downstream of the reaction zone in plug flow. There is a distinct gap or dark space of ∼1 mm between the burner face and the

bases of the luminous reaction-zone cones on each hypodermic tube. This gap corresponds to the preheat region of the flame before major chemical reaction takes place. Since hydrogen flames contain very little natural ionization, ions were introduced by spraying a dilute aqueous solution of CsCl as an aerosol into the premixed flame gas using a pneumatic atomizer [14] to produce Cs^+ by thermal (collisional) ionization of the resulting free atoms of Cs. Roughly speaking, the amounts of Cs and Cl in flame 2 when spraying 10^{-4} M CsCl solution were small ($\sim 10^{-9}$ mol fraction). Negative ions including Cl^- could not be detected with the mass spectrometer although the same concentration of total cesium from CsCl yields a large Cs^+ signal. Alternatively, the addition of a very small metered flow of methane CH_4 produced H_3O^+ ions by chemi-ionization. When desired, negative Cl^- ions along with H_3O^+ could be produced in the flame by the addition of C_2HCl_3 vapour from a gas saturator maintained at 0 °C [15]; part of the diluent nitrogen was employed as the carrier gas through the saturator. The halocarbon was added to give a total Cl concentration in the burnt gas in the range 0.0004–0.004 mol fraction.

3. Theory and background

The equations governing the flux Γ of charged particles in the flame toward the nozzle are

$$\Gamma_e = n_e v_f + n_e \mu_e \nabla\varphi - D_e \nabla n_e \quad (1)$$

$$\Gamma_+ = n_+ v_f - n_+ \mu_+ \nabla\varphi - D_+ \nabla n_+ \quad (2)$$

$$\Gamma_- = n_- v_f + n_- \mu_- \nabla\varphi - D_- \nabla n_- \quad (3)$$

where n is the particle density (i.e. concentration), v_f is the flow velocity in the burnt gas, μ is mobility, and D is the diffusivity (diffusion coefficient); the subscripts e, $+$, and $-$ refer to electrons, positive ions, and negative ions, respectively. On the right-hand side of each equation, the first term denotes convection (flow), the second is mobility, and the third represents diffusion. In terms of the potential gradient, the electric field is given by $E = -\nabla\varphi$. The fluxes are converted to currents when multiplied through by eA, where e is the electronic charge and A is the cross-sectional area of the flame.

For discussion of the i–V characteristics, an approximate set of values is needed. For the electron, $\mu_e = 0.4\ m^2\ V^{-1}\ s^{-1}$ [16] and $\mu_+(H_3O^+) = 8 \times 10^{-4}\ m^2\ V^{-1}\ s^{-1}$ for a flame plasma at 1 atm [17]. At constant thermal energy, $\mu \propto 1/M^{1/2}$. Based on the H_3O^+ value, $\mu_+(Cs^+) = 2.9 \times 10^{-4}$ and $\mu_-(Cl^-) = 5.7 \times 10^{-4}\ m^2\ V^{-1}\ s^{-1}$. With the atomizer spraying a 1.00×10^{-4} M solution of CsCl, complete ionization of the Cs gives $n_+ \sim 4 \times 10^{15}$ ions m^{-3}; the value will be determined below. This magnitude of the ion density is large enough for ambipolar diffusion of the electrons and positive ions (Cs^+ or H_3O^+) to operate [18]. Because the flame plasma is isothermal, the Einstein relation can be employed to estimate the free diffusion coefficients: $D_e/\mu_e = D_+/\mu_- = D_-/\mu_- = RT/eN_a$, where R is the gas constant and N_a is the Avogadro number. If negative ions are not present, the ambipolar diffusion coefficient is $D_a \simeq 2D_+$. Assuming that radial diffusion can be neglected, the cross-sectional area A of the flame in the burnt gas is determined from $\dot{V}T_f/rT_r = Av_f$ giving $A = 1.05 \times 10^{-4}\ m^2$ for room temperature $T_r = 295.15$ K (see Table 1). Here, $\dot{V}$ is the volumetric flow rate of the unburnt gas mixture at T_r and r is the ratio of the number of moles of reactants in the unburnt gas to the number of moles of products in the burnt gas at flame temperature T_f. With these values, it is possible to give a reasonably quantitative analysis of the measurements below. Calculations will be carried out to a precision of two or three digits for comparison of the relative magnitudes, but any calculation involving mobilities μ is accurate to one significant figure at best.

When interpreting new results, it is useful to consider Fig. 2 which sketches the variations of electric potential between the burner and nozzle when $\Delta\varphi$ is positive, negative, or near zero. It is based on our previous, but very qualitative, work [7] and has been modified in the light of the present studies. When $\Delta\varphi$ is appreciably positive, there is interestingly a significant ohmic voltage drop in the bulk flame plasma [8,9] and a relatively large jump in

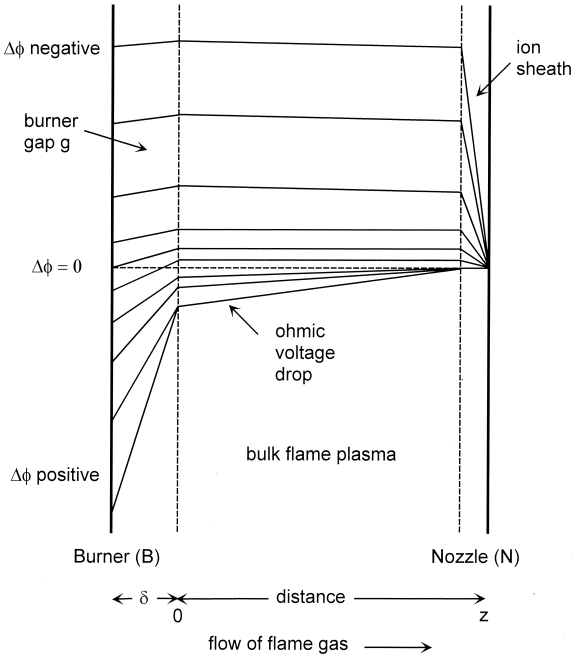

Fig. 2. Sketch of the potential distribution between the burner and the nozzle electrode at a fixed axial distance z for a variety of applied potentials $\Delta\varphi$. The drawing is not to scale; large values of $\Delta\varphi$ are underscaled relative to those near $\Delta\varphi = 0$, and the burner gap is very much thicker than the ion sheath at the nozzle. The sketch approximates the H_3O^+/e^- flame plasma depicted in Figs. 5 and 6.

potential across the dark space or gap adjacent to the burner's surface. The consequence is that positive ions in the bulk flame are slowed down or retarded slightly, but the major factor is the increased attraction of positive ions to the burner due to the large potential gradient across the burner gap. In contrast, the drift velocity of the electrons toward the nozzle increases only slightly above the flow velocity v_f in the ohmic voltage drop (positive potential gradient); the reason is that the electron flux is limited by the rate of production of electrons/ions in the flame reaction zone. Although the fluxes of positive ions and electrons are different, their concentrations are equal to one another at any point z in the bulk flame, i.e. quasi-neutrality is preserved. The current through the flame is maintained by positive ions being attracted to the burner and otherwise by an equal net current of electrons (and negative ions, if present) to the nozzle.

When $\Delta\varphi = 0$, the bulk flame gas is maintained at a slightly elevated space potential because there is an ion sheath at the nozzle and a positive potential gradient across the burner gap which behaves like an ion sheath. A constant space potential has been drawn in Fig. 2 for $\Delta\varphi = 0$. Depending on the additive, however, the ion concentration in the bulk flame gas might either increase or decrease downstream because of a net generation or recombination of positive ions, respectively. This would give rise to a small potential gradient in the bulk flame which is positive for generation or negative for recombination. When $\Delta\varphi$ is appreciably negative, on the other hand, there is a thin ion sheath covering the nozzle. Electrons are light enough to be stopped by the potential gradient in this ion sheath. With increasing negative voltage, a slight negative potential gradient builds up in the bulk flame plasma sufficient to hold the electrons stationary. The nozzle collects a positive ion current governed by convection in the bulk flame. At the burner, the positive potential gradient similar to an ion sheath is maintained but its magnitude decreases as $\Delta\varphi$ becomes increasingly negative. The burner must collect a net electron current equivalent to the ion current at the nozzle, but the electrons have to surmount the repulsive potential gradient across the burner gap. These distributions of electric potential can be refined and made more quantitative in the light of new experimental measurements.

4. Results and discussion

4.1. Flame plasma with Cs^+/e^-

Fig. 3 presents an i–V characteristic measured at $z = 20$ mm downstream with $\Delta\varphi$ in the range from -50 to $+50$ V when the atomizer was spraying a 1.00×10^{-4} M aqueous solution of CsCl. Other useful measurements presented below are profiles of current i versus axial distance z at a fixed value of $\Delta\varphi$. Fig. 4(a) shows such a profile for the positive ion current i_+(N) collected by the nozzle N with $\Delta\varphi = -50$ V; Fig. 4(b) is the electron current i_e(N) with $\Delta\varphi = +50$ V. Since no negative ions are present,

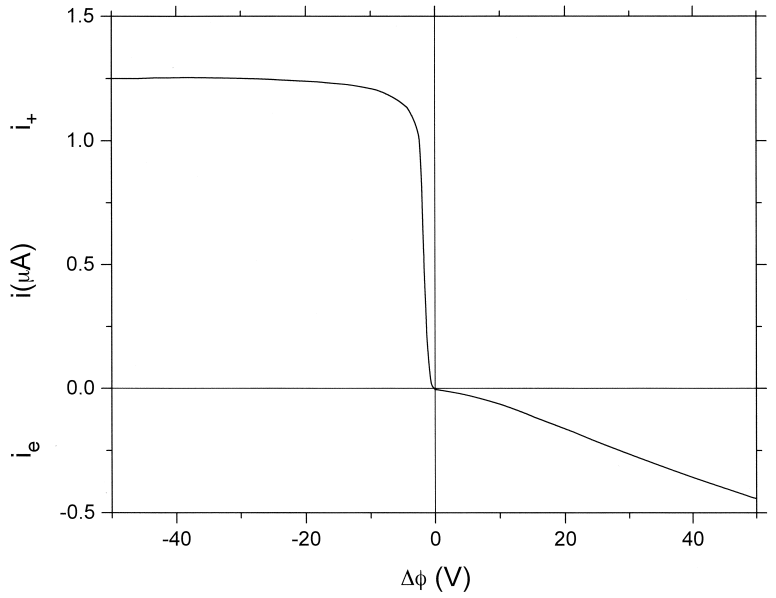

Fig. 3. Current–voltage characteristic of the flame doped with the atomizer spraying a 1.00×10^{-4} M solution of CsCl to give a Cs^+/e^- plasma measured at $z = 20$ mm downstream.

quasi-neutrality of the flame plasma requires that $n_+ = n_e$ at any point z on the flame axis. With $\Delta\varphi$ negative, $i_+(\mathrm{N}) = -i_e(\mathrm{B})$, the electron current at the burner B, and with $\Delta\varphi$ positive, $i_e(\mathrm{N}) = -i_+(\mathrm{B})$ because the nozzle and burner must always collect currents of equal magnitude but opposite sign. All of the figures are presented from the point of view of current collection by the nozzle N. Finally, it should be recognized that, because ion concentrations in general change along the length of a flame, $n_+(\mathrm{N}) = n_e(\mathrm{N}) \neq n_+(\mathrm{B}) = n_e(\mathrm{B})$, i.e. the charge densities n at the nozzle and burner are not the same.

Before going further, it should be clearly understood that the nozzle does not function as a conventional Langmuir probe [19]. In general, the space potential of a bulk plasma is fixed by the potential on one conducting wall of relatively large area in contact with the plasma. A Langmuir probe is introduced in the form of a tiny conducting electrode (cylindrical in the form of a short wire, spherical or planar) whose potential may be biased positive or negative to collect electrons or positive ions, respectively. The probe's area must be very small compared with the area of the wall so that variation of the Langmuir probe potential

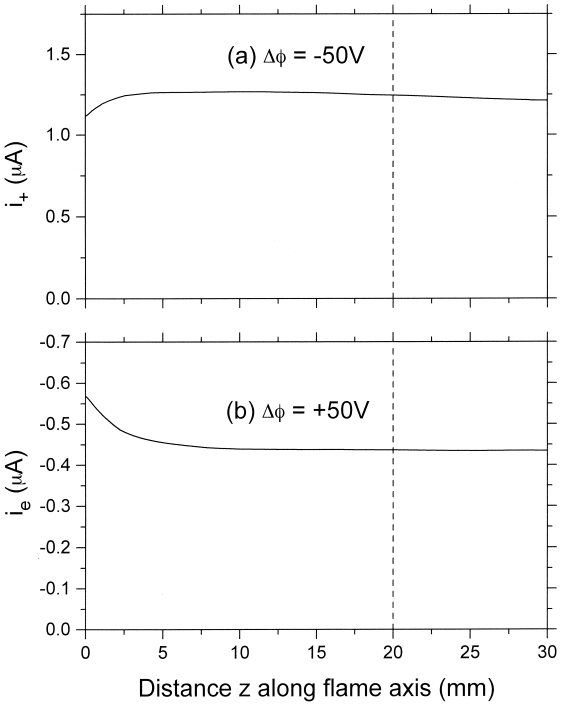

Fig. 4. Current profiles along the flame axis z with (a) $\Delta\varphi = -50$ V, and (b) $\Delta\varphi = +50$ V for the same flame plasma presented in Fig. 3.

does not change the plasma space potential. In the present case, the nozzle and the burner function as two comparable "walls"; both can have a major influence in determining the electrical properties of the bulk flame plasma.

Returning to Fig. 3, consider first the left-hand side where $\Delta\varphi$ is negative. In the first few volts, electrons are increasingly repelled by the nozzle electrode which is covered by an ion sheath, but positive Cs^+ ions carry on with the flow and are collected by the nozzle to yield a net positive current. To stop electrons moving with the drift velocity requires a potential gradient $\nabla\varphi \simeq -E_{\mathrm{crit}(i)} = v_f/\mu_e = 19.8/0.4 = 50\ \mathrm{V\ m^{-1}}$; it is equivalent to a critical electric field just sufficient to hold electrons stationary against the flow velocity v_f. To stop these electrons in $z = 20$ mm of flame plasma would require a potential difference of 1.0 V. Of course, to stop all the electrons requires rather more voltage, because the electrons have a thermal velocity distribution superimposed on v_f. When all the electrons are repelled, the nozzle collects a constant saturation ion current

$$i_+(\mathrm{N}) = eAn_+(\mathrm{N})v_f \tag{4}$$

The potential across the ion sheath grows in proportion to the magnitude of the applied voltage. Thus, when $\Delta\varphi$ is appreciably negative, Eq. (2) for positive ions is dominated by the convection term; the contribution from mobility is much smaller and diffusion is negligible [7–9]. A novel and important application is immediately apparent. If the flame of diameter d is well-characterized such that $A = \pi d^2/4$ and v_f are known or can be reasonably estimated, the absolute ion density can be determined by simply measuring the current to the burner or nozzle. In the present case where $i_+(\mathrm{N}) = 1.25\ \mu\mathrm{A}$, $n_+(\mathrm{N}) = 3.7 \times 10^{15}$ ions $\mathrm{m^{-3}}$, using values from Table 1 in Eq. (4). Such a value of $n_+(\mathrm{N})$ is accurate to ~3% and so is more precise than a mass-spectrometric measurement with errors of ~10%–20%.

Fig. 4(a) with $\Delta\varphi = -50$ V essentially traces out a profile of $n_+(\mathrm{N}) = n_e(\mathrm{N}) = i_+(\mathrm{N})/eAv_f$. Ions are produced by thermal ionization of Cs atoms [20]

$$\mathrm{CS} + \mathrm{M} \rightarrow \mathrm{Cs^+} + e^- + \mathrm{M} \tag{5}$$

where M is any flame species. The process causes the ion density to rise in the reaction zone, reaching equilibrium near $z = 4$ mm downstream, corresponding to a time of 0.20 ms. This suggests that the time constant for thermal ionization is $\sim 0.20 \times (1 - 1/e) = 0.13$ ms; i.e. $1/k_5[\mathrm{M}] \simeq 0.13$ ms, with k_5 being the rate constant for thermal ionization of Cs at 2400 K. This gives $k_5 \simeq 2.6 \times 10^{-15}\ \mathrm{cm^3\ molecule^{-1}\ s^{-1}}$, in reasonable agreement with the literature value of $3.3 \times 10^{-15}\ \mathrm{cm^3\ molecule^{-1}\ s^{-1}}$ [20]. The drop in ion density at $z = 0$ can be used to estimate the ion or electron density at the burner, since $n_+(\mathrm{N})_0 \simeq n_+(\mathrm{B}) = n_e(\mathrm{B})$; the resulting slightly lower value, $n_+(\mathrm{B}) = 3.3 \times 10^{15}$ ions $\mathrm{m^{-3}}$, refers to the density near the dark gap separating the luminous reaction zone from the burner face. This estimate of $n_+(\mathrm{B})$ will be refined in the next section.

For saturation at the left in Fig. 3, the burner must collect an equal electron current $i_e(\mathrm{B}) = -i_+(\mathrm{N})$ against the repulsive potential gradient $\nabla\varphi_g$ across the burner gap g (see Fig. 2). The gradient can be represented by $\nabla\varphi_g = \Delta\varphi_g/\delta$, where $\Delta\varphi_g$ is the potential across the gap thickness $\delta \approx 1$ mm (as will be deduced later). The current is given by

$$i_e(\mathrm{B}) = eA(\bar{u}_e/4)n_e(\mathrm{B}) \exp(-e\Delta\varphi_g/kT) \tag{6}$$

in terms of the surface flux from kinetic theory, modified by the Boltzmann factor for the repulsive potential [21]; here, $\bar{u}_e$ is the mean speed of the electrons at temperature T. As the magnitude of $\Delta\varphi$ increases, $\Delta\varphi_g$ decreases (see Fig. 2) and more electrons reach the burner. In fact, the gap temperature is much lower than the flame temperature of 2400 K. Nevertheless, it is this expression for $i_e(\mathrm{B})$ which controls the rise of the characteristic up to the saturation plateau on the left. In summary, nearly all of the applied voltage $\Delta\varphi = -50$ V appears as a drop in potential across the ion sheath at the nozzle, with very little across the burner gap and ~1 V in the bulk flame. In general, the saturation value of the characteristic for $\Delta\varphi < 0$ is controlled by the electrons near the nozzle which must be progressively retarded and stopped, but the rise to saturation is controlled by the flow of electrons to the burner.

Consider next the right-hand side of Fig. 3 where $\Delta\varphi$ becomes increasingly positive from 0 to +50 V. The bulk flame plasma sustains a small positive potential gradient (see Fig. 2) which has a negligible retardation effect on the heavy positive ions. Initially, it might be thought that this potential gradient would cause the mobile electrons to speed up, giving them a drift velocity $>v_f$. However, the electron drift velocity is limited to v_f by the rate of production of electrons (and positive ions) in the flame reaction zone. In fact, the electron current to the nozzle is limited by the flow of positive ions to the burner across the burner gap δ against the convective flow of the flame

$$i_e(\mathrm{N}) = -i_+(\mathrm{B}) = -eAn_+(\mathrm{B})\mu_+\nabla\varphi_g \qquad (7)$$

where $\nabla\varphi_g = \Delta\varphi_g/\delta$. With $\Delta\varphi = +50$ V and $n_+(\mathrm{B}) = 3.3 \times 10^{15}$ ions m^{-3} derived above from Fig. 4(a), the measured current $i_e(\mathrm{N}) = -0.45$ μA in Fig. 3 requires a potential gradient $\nabla\varphi_g = 2.74 \times 10^4$ V m^{-1}. Above $\sim +5$ V in Fig. 3, the growth of $i_e(\mathrm{N}) = -i_+(\mathrm{B})$ is remarkably linear; the measured inverse slope of the i–V characteristic can be interpreted as the electrical resistance of the gap $R_g = \Delta\varphi_g/i_+(\mathrm{B}) = 105$ MΩ. This gives $\Delta\varphi_g = 47.25$ V, with $\Delta\varphi_f = 50 - 47.25 = 2.75$ V across $z = 20$ mm of bulk flame, and $\nabla\varphi_f = 138$ V m^{-1}. It is clear that most of the applied voltage appears across the burner gap. Also, an estimate can be obtained for the gap thickness $\delta = \Delta\varphi_g/\nabla\varphi_g = 1.7$ mm; physically, it might include the visible dark gap and the base of the reaction-zone flame cones. Alternatively, the ohmic resistance is given by the standard formulation $R_g = \delta/c_+A$, where $c_+ = en_+(\mathrm{B})\mu_+ = 1.6 \times 10^{-7}$ Ω^{-1} m^{-1} is the electrical conductivity with positive ions as the charge carrier.

The resistance of the bulk flame R_f can be found at $\Delta\varphi = +50$ V because $R_f = \Delta\varphi_f/i_+(\mathrm{B}) = 2.75/0.45 \times 10^{-6} = 6.1$ MΩ. Also, $\nabla\varphi_f = \Delta\varphi_f/z = 1.4 \times 10^2$ V m^{-1} is the potential gradient in the bulk flame, with the voltage $\Delta\varphi_f$ appearing across the axial distance $z = 20$ mm. Because the current flowing through the flame is constant everywhere, the total applied voltage $\Delta\varphi$ divides in the ratio $\Delta\varphi_g/\Delta\varphi_f = R_g/R_f$. It is probably safe to assume that $R_f \propto z$, where z is the flame length. If this is the case, $\Delta\varphi_f \propto R_f$ and $R_f \propto z$ so that the potential gradient in the bulk flame $\nabla\varphi_f = \Delta\varphi_f/z$ is constant, independent of z. This point will be elaborated and proven in Sec. 4.2.

In Fig. 4(b) with $\Delta\varphi = +50$ V, Eq. (7) predicts that the profile should be constant, independent of z, because $n_+(\mathrm{B})$ is constant when the rate of ion production is constant. However, $i_e(\mathrm{N}) = -i_+(\mathrm{B}) = \Delta\varphi/(R_f + R_g)$; as $z \to 0$, $R_f \to 0$ causing $i_e(\mathrm{N})$ to increase as observed in Fig. 4(b). Further, the constancy of $\nabla\varphi_g$ breaks down when z is small; $\nabla\varphi_f$ now invades or interferes with $\nabla\varphi_g$ in the burner gap causing it to increase, with a resulting increase in the magnitude of $i_e(\mathrm{N})$. The resistance expression also shows why the i–V characteristic in Fig. 3 is linear: since $R_f \ll R_g$ and R_g is constant, $i_e(\mathrm{N}) \propto \Delta\varphi$.

For $\Delta\varphi = +50$ V, $\nabla\varphi_g = 2.74 \times 10^4$ V m^{-1} $< -E_{\mathrm{crit}(e)} = \nu_f/\mu_+ = 6.72 \times 10^4$ V m^{-1}, the critical electric field required to stop the massive Cs^+ positive ions; this is the condition normally associated with the formation of an electron sheath at the nozzle. That $\nabla\varphi_g < -E_{\mathrm{crit}(e)}$ explains why the characteristic in Fig. 3 does not bend over and saturate for $\Delta\varphi \leq +50$ V. For saturation to occur, all of the positive ions formed in the reaction zone must be pulled back and collected by the burner as they are generated. Even without saturation, the general principle for $\Delta\varphi > 0$ is clear: the shape of the characteristic is controlled by the flow of positive ions to the burner.

4.2. Flame plasma with H_3O^+/e^-

Fig. 5 gives an i–V characteristic with the atomizer switched off, but with the same flame doped with methane (mol fraction $= 4.00 \times 10^{-4}$) at a constant distance $z = 20$ mm downstream. The only flame ion present is H_3O^+, formed mainly by the well-known chemi-ionization reaction for hydrocarbon flames [22,23]

$$\mathrm{CH} + \mathrm{O} \rightarrow \mathrm{HCO}^+ + e^- \qquad (8)$$

followed by proton transfer to water, a major product downstream

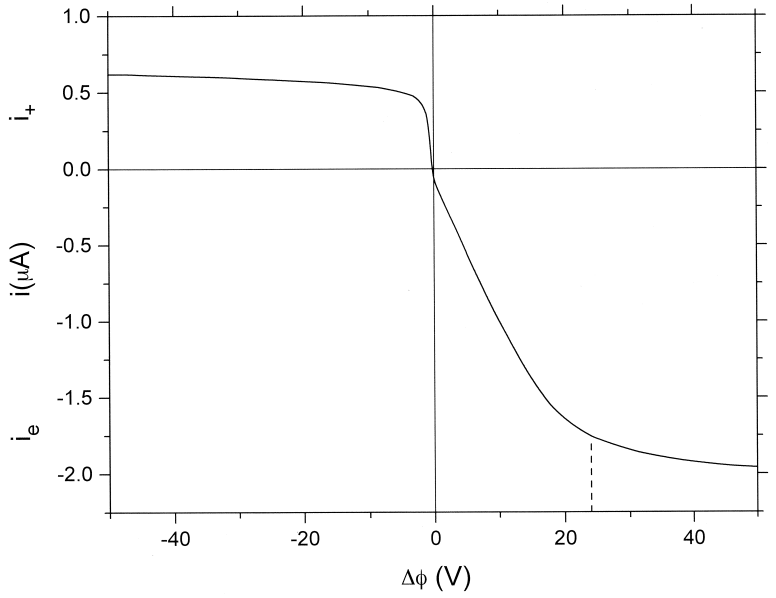

Fig. 5. Current–voltage characteristic of the flame doped with 0.0004 mol fraction of methane in the burnt gas to give an H_3O^+/e^- plasma measured at $z = 20$ mm downstream.

$$HCO^+ + H_2O \rightarrow H_3O^+ + CO \quad (9)$$

The characteristic is similar to that in Fig. 3 with two major differences: at positive $\Delta\varphi$, i_e(N) now appears to saturate; also, it has a magnitude considerably greater than the saturation value of i_+(N) at negative $\Delta\varphi$. Fig. 6 gives profiles under the same flame conditions for $z = 0$–30 mm with (a) $\Delta\varphi = -50$ V and (b) $\Delta\varphi = +50$ V. For the explanation of Fig. 5, it is first necessary to know the distribution of H_3O^+ ions along the flame. The distribution is given by the plot in Fig. 6(a) where convective flow dominates, so the saturation ion current $i_+(\mathrm{N}) = eAn_+(\mathrm{N})v_f$ throughout the burnt gas, i.e. $i_+(\mathrm{N}) \propto [H_3O^+]$. As expected, the profile confirms that reactions (8) and (9) produce H_3O^+ in the reaction zone near $z = 0$ far above its equilibrium concentration; the ions subsequently decay downstream throughout the burnt gas by electron–ion recombination [24]

$$H_3O^+ + e^- \rightarrow H + H + OH \quad (10)$$

This picture is confirmed by plotting $1/i_+$(N) from Fig. 6(a) versus z. Such a recombination plot (not shown here) is a good straight line indicating a

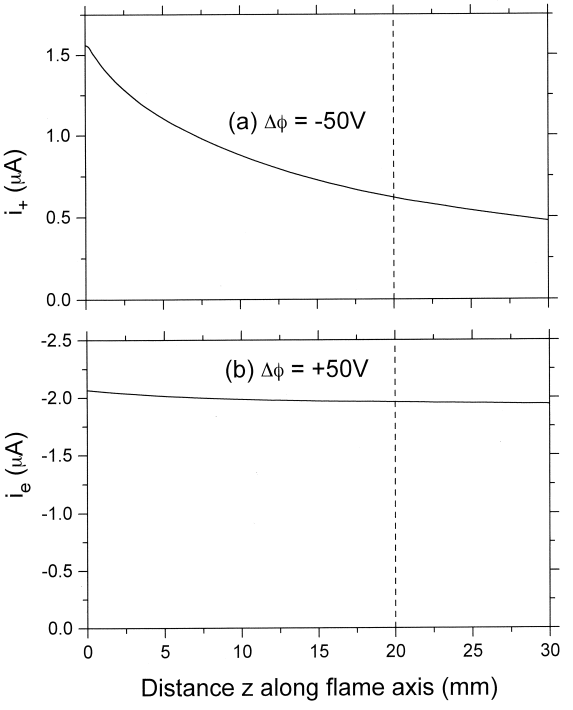

Fig. 6. Current profiles along the flame axis z with (a) $\Delta\varphi = -50$ V, and (b) $\Delta\varphi = +50$ V for the same flame plasma presented in Fig. 5.

recombination coefficient for reaction (10) of 3.1×10^{-7} cm^3 molecule^{-1} s^{-1} at 2400 K. This agrees well with the literature value of 2.9×10^{-7} cm^3 molecule^{-1} s^{-1} [24]. More importantly, such good agreement confirms that charge neutrality (i.e. $[e^-] = [H_3O^+]$) is not upset by the application of $\Delta\varphi = -50$ V.

The detailed analysis of Fig. 5 for $z = 20$ mm downstream, including the saturation behaviour at positive $\Delta\varphi$, can be accomplished in ten consecutive steps. First, $i_+(\mathrm{N}) = 0.62$ μA at $\Delta\varphi = -50$ V is substituted in Eq. (4) to calculate $n_+(\mathrm{N}) = n_e(\mathrm{N}) = 1.86 \times 10^{15}$ m^{-3}. The rest of the analysis involves the case where $\Delta\varphi$ is positive. Second, the resistance of $z = 20$ mm of bulk flame is calculated from the standard formulation $R_f = z/en_e(\mathrm{N})\mu_e A = 1.60$ MΩ. This is valid because electrons are the only charge carrier to the nozzle; it was not true in the case of the Cs plasma. Third, the potential across the bulk flame is obtained from $\Delta\varphi_f = R_f i_e(\mathrm{N}) = 3.11$ V using the saturation current $i_e(\mathrm{N}) = -1.95$ μA at +50 V. Fourth, the potential gradient in the bulk flame is given by $\nabla\varphi_f = \Delta\varphi_f/z = 156$ V m^{-1} where z refers to 20 mm of flame. Now, $i_e(\mathrm{N})$ is observed in Fig. 5 to saturate (or nearly so), i.e. it comes to a constant value of –1.95 μA at $\Delta\varphi = +50$ V. Recall from the previous section that the current at positive $\Delta\varphi$ is controlled by the flow of positive ions to the burner. Saturation can occur only if the entire production of positive ions formed in the reaction zone is attracted back to the burner. Thus, fifth, saturation requires a potential gradient across the burner gap $\nabla\varphi_g = v_f/\mu_+ = 2.48 \times 10^4$ V m^{-1} for H_3O^+ ions. As a consequence, sixth, $n_+(\mathrm{B}) = 5.83 \times 10^{15}$ ions m^{-3} is obtained from $i_+(\mathrm{B}) = -i_e(\mathrm{N}) = eAn_+(\mathrm{B})\mu_+\nabla\varphi_g = eAn_+(\mathrm{B})v_f = 1.95$ μA at saturation. Seventh, the experimental resistance of the burner gap $R_g = 10.7$ MΩ is measured from the inverse slope of the i–V characteristic. Eighth, the thickness of the burner gap $\delta = 0.84$ mm is calculated from $R_g = \delta/en_+(\mathrm{B})\mu_+ A$. Ninth, the potential across the burner gap is obtained from $\Delta\varphi_g = \delta \times \nabla\varphi_g = 20.9$ V. Finally, tenth, the voltage at which saturation occurs for $\Delta\varphi > 0$ is found from $\Delta\varphi(\mathrm{sat}) = \Delta\varphi_f + \Delta\varphi_g = 24.0$ V. This is the value indicated by the dashed line in Fig. 5. In fact, Fig. 5 shows that a little more voltage is required for saturation to stop the more energetic positive ions for collection by the burner. Even so, Fig. 5 shows that H_3O^+ ions can be fully retarded with $\Delta\varphi = +50$ V, whereas from Fig. 3 an applied potential of this magnitude failed to prevent some of the heavier Cs^+ ions from reaching the nozzle.

Further details of the potential distribution sketched in Fig. 2 are now apparent. The potentials are approximately representative of those present in the flame plasma whose i–V characteristic is given in Fig. 5. The gradients have been drawn to meet at a sharp point at the edges of the burner gap and nozzle sheath; in reality, the potentials would be rounded at these corners to allow for the existence of a presheath. For illustrative purposes, not all of the potential gradients are drawn to scale. The lowest potentials in Fig. 2 with $\Delta\varphi > 0$ have been drawn to illustrate saturation; presumably additional applied voltage above that required to achieve saturation simply adds across the burner gap.

An estimate of $n_+(\mathrm{B}) = 4.70 \times 10^{15}$ ions m^{-3} can be obtained from Fig. 6(a) using the peak value $i_+(\mathrm{B}) = eAn_+(\mathrm{B})v_f = 1.57$ μA for $z = 0$ at $\Delta\varphi = -50$ V. This was done out of necessity in analyzing Fig. 3 for the Cs plasma, because the characteristic did not saturate at positive $\Delta\varphi$. It is substantially lower than the alternative value of $n_+(\mathrm{B}) = 5.83 \times 10^{15}$ ions m^{-3} determined in the previous paragraph from saturation at $\Delta\varphi = +50$ V. The reason is that the lower value is derived from the maximum in i_+ just discernible in Fig. 6(a), which represents a local balance or equality of the rates of ion production and ion loss. The higher value captures the total ion production or yield, but without loss, near the upstream edge of the reaction zone. It is possible that HCO^+ as well as H_3O^+ ions are involved. This would only decrease the value of μ_+ from 8×10^{-4} for H_3O^+ to $\sim 6.3 \times 10^{-4}$ m^2 V^{-1} s^{-1} for HCO^+ and so not affect the above conclusion. Here, then, is a way of removing the positive chemi-ions produced early in the reaction zone and also of measuring how many have been generated without any loss by recombination, e.g. in reaction (10). The accuracy of this

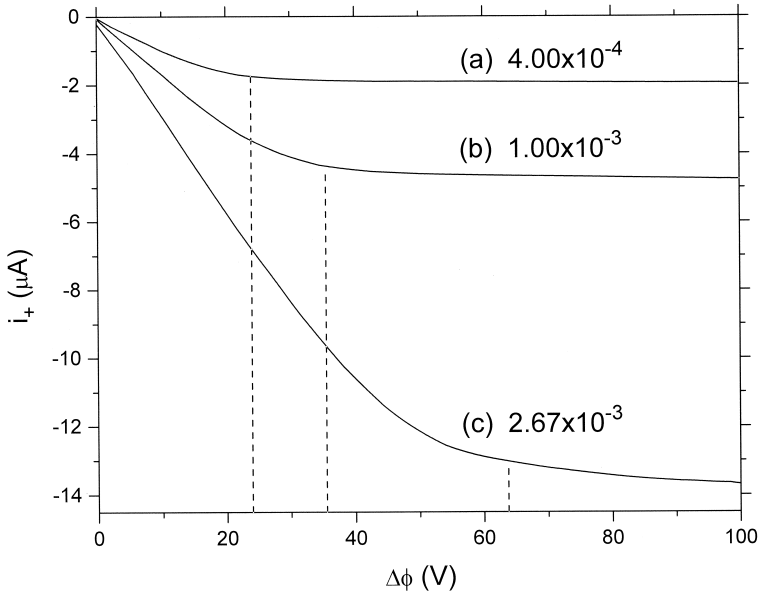

Fig. 7. Current–voltage characteristics of the flame at positive $\Delta\varphi$ for methane concentrations of (a) 4.00×10^{-4}, (b) 1.00×10^{-3} and (c) 2.67×10^{-3} mole fraction in the burnt gas to give H_3O^+/e^- plasmas measured at $z = 20$ mm downstream.

measurement is better than ±10% and so is a great improvement on mass-spectrometric determinations of a concentration in the reaction zone; these are at best good to a factor of 2 because the local temperature is uncertain.

Fig. 6(b) now requires further explanation because of its lack of similarity to Fig. 6(a). Fig. 6(b) presents a profile of $i_e(\mathrm{N}) = -i_+(\mathrm{B})$ versus z at constant $\Delta\varphi = +50$ V which is almost flat. The equation of the profile is given by

$$i_e(\mathrm{N}) = \frac{\Delta\varphi}{R_f + R_g} = \frac{\Delta\varphi}{\dfrac{z}{en_e(\mathrm{N})\mu_e A} + \dfrac{\delta}{en_+(\mathrm{B})\mu_+ A}} \tag{11}$$

If the resistances of the bulk flame and burner gap (see Fig. 2) are such that $R_f \ll R_g$, then $\Delta\varphi_f \ll \Delta\varphi_g$, so that $\Delta\varphi \simeq \Delta\varphi_g$; thus, $i_e(\mathrm{N}) = eAn_+(\mathrm{B})\mu_+\nabla\varphi_g \simeq eAn_+(\mathrm{B})\mu_+\Delta\varphi/\delta$. This shows that the electron current to the nozzle is controlled by the flow of less mobile positive ions to the burner across the burner gap, as previously stated. It also shows that, with $R_f \ll R_g$, the first term in the denominator of Eq. (11) can be neglected, so $i_e(\mathrm{N})$ is independent of z giving the nearly constant profile in Fig. 6(b). In general, $R_f < R_g$; e.g. their respective values are 1.6 and 10.7 MΩ in the present case. Fig. 6(a) shows that $n_e(\mathrm{N})$ decreases with increasing z. Therefore, it is expected from Eq. (11) that $i_e(\mathrm{N})$ will decrease slightly with increasing z as is observed in Fig. 6(b).

Fig. 7 illustrates the effect on saturation at positive $\Delta\varphi$ of increasing the H_3O^+ concentration by raising the concentration of the methane additive. The i–V characteristics were measured at $z = 20$ mm downstream for CH_4 mole fractions of 4.00×10^{-4}, 1.00×10^{-3}, and 2.67×10^{-3} and for $\Delta\varphi$ up to +100 V to achieve saturation in all three cases. The different saturation currents at $\Delta\varphi = -50$ V were also measured (not shown in Fig. 7) for these three characteristics. Each characteristic was analyzed by the ten steps outlined above, and all the results are given in Table 2. In all three cases it is seen that $\Delta\varphi_f < \Delta\varphi_g$ for $\Delta\varphi > 0$. Also, Table 2 shows that the saturation values of $n_+(\mathrm{B})$ at positive $\Delta\varphi$, representative of the total ion yield, are approximately proportional to the CH_4 concentration; this is expected from chemi-ionization by reaction (8) and the fact that the concentration of CH radicals is proportional to the

Table 2
Analysis of the i–V characteristics in Fig. 7 for $z = 20$ mm downstream

Quantity	Methane concentration (mole fraction)		
	0.000400	0.00100	0.00267
$i_+(\mathrm{N}) = -i_e(\mathrm{B})$ at -50 V (μA)	0.62	0.75	0.89
$n_+(\mathrm{N}) = n_e(\mathrm{N})$ (m^{-3})	1.86×10^{15}	2.24×10^{15}	2.66×10^{15}
R_f (MΩ)	1.60	1.32	1.11
$i_e(\mathrm{N}) = -i_+(\mathrm{B})$ at $+100$ V (μA)	-1.95	-4.77	-13.65
$\Delta\varphi_f$ (V)	3.11	6.30	15.2
$\nabla\varphi_f$ (V m^{-1})	156	315	759
$\nabla\varphi_g$ for saturation (V m^{-1})	2.48×10^4	2.48×10^4	2.48×10^4
$n_+(\mathrm{B}) = n_e(\mathrm{B})$ (m^{-3})	5.83×10^{15}	14.3×10^{15}	40.8×10^{15}
R_g (MΩ)	10.7	6.13	3.56
Gap thickness δ (mm)	0.84	1.18	1.96
$\Delta\varphi_g$ (V)	20.9	29.2	48.6
$\Delta\varphi(\mathrm{sat}) = \Delta\varphi_f + \Delta\varphi_g$ (V)	24.0	35.5	63.8

quantity of CH_4 added. Fig. 7 shows that the values of $\Delta\varphi$(sat) required to produce saturation of the characteristic at positive $\Delta\varphi$ (dashed lines) also increase with increasing CH_4 concentration. This derives from the calculated thickness δ of the burner gap (see Table 2) increasing when more CH_4 is added. The result is that a larger applied voltage is necessary to produce the critical voltage gradient $\nabla\varphi_g = \nu_f/\mu_+$. An explanation might involve the burning velocity S_u; hydrogen has the highest value of any fuel and methane has the lowest value of the hydrocarbons [25]. Since the position of the luminous reaction zone on the burner face represents a balance of the unburnt gas flow velocity forwards and S_u backwards, the introduction of even a small amount of methane into the hydrogen fuel can produce a significant reduction of S_u and a concomitant increase of δ for this flame. An alternative way of expressing this is that with more CH_4 added, the location of the maximum rate of ion production shifts slightly downstream.

4.3. Flame plasma with $H_3O^+/Cl^-/e^-$

Fig. 8 shows two i–V characteristics measured at $z = 20$ mm downstream for the flame doped with (a) C_2HCl_3 to give 0.00400 mole fraction of total chlorine, and consequently 0.00267 mole fraction of total carbon also, in the burnt gas and (b) 0.00267 mole fraction of CH_4 to give the same total carbon concentration as the chlorine-doped flame. Chlorine exists in this fuel-rich flame almost entirely as HCl and atomic Cl which are linked by the balanced reaction [26]

$$\mathrm{HCl} + \mathrm{H} \rightleftarrows \mathrm{Cl} + \mathrm{H_2} \tag{12}$$

A comparatively small concentration of negative Cl^- ions is produced by the reaction

$$e^- + \mathrm{HCl} \rightleftarrows \mathrm{Cl^-} + \mathrm{H} \tag{13}$$

which is fast and also balanced [26]. At this level of total chlorine in this particular flame, the calculated equilibrium mol fractions of HCl and Cl, based on the JANAF Tables [27], are 0.00388 and 0.000116, respectively, and the ratio $[Cl^-]/[e^-] = 4.70$. From the saturation value at $\Delta\varphi = -50$ V for Fig. 8(a), $n_+(\mathrm{N}) = 5.59 \times 10^{15}$ m^{-3} so that $n_e(\mathrm{N}) = 0.98 \times 10^{15}$ m^{-3} and $n_-(\mathrm{N}) = 4.61 \times 10^{15}$ m^{-3} for Cl^-. For Fig. 8(b), $n_+(\mathrm{N}) = n_e(\mathrm{N}) = 2.66 \times 10^{15}\,\mathrm{m}^{-3}$ as in Table 2.

In Fig. 9, curves (a) and (b) give profiles for $\Delta\varphi = -50$ V in the range $z = 0$–30 mm for the same two additive cases given in Fig. 8. It is clear that the recombination rate is slower in curve (a) when roughly 82% of the free electrons are replaced by negative Cl^- ions compared with curve (b). This follows from the fact that the rate coefficient for the ion–ion recombination reaction [28]

$$\mathrm{H_3O^+} + \mathrm{Cl^-} \rightarrow \mathrm{H_2O} + \mathrm{HCl} \tag{14}$$

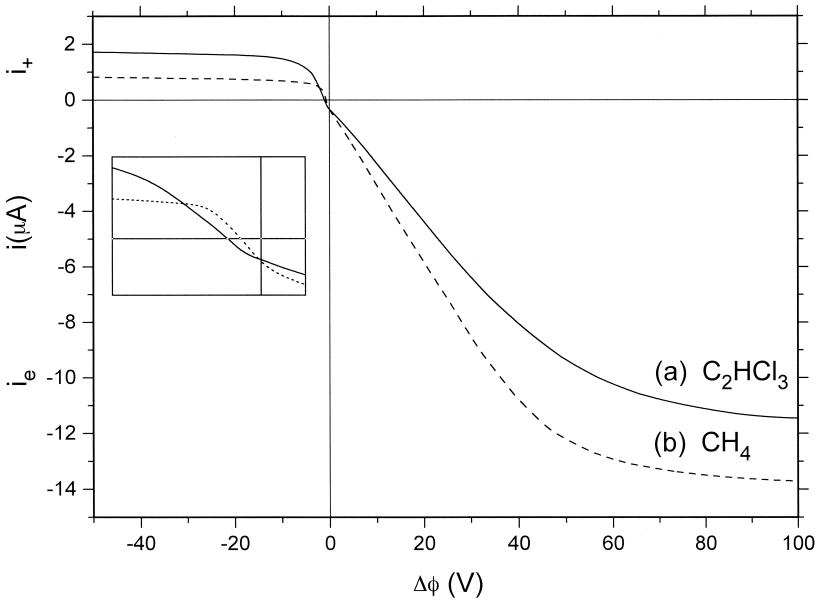

Fig. 8. Current–voltage characteristics of the flame doped with (a) C_2HCl_3 to give an $H_3O^+/Cl^-/e^-$ plasma and (b) CH_4 to give an H_3O^+/e^- plasma having the same mole fraction of carbon = 0.00267 in the burnt gas, measured at $z = 20$ mm downstream. The inset expands the details of the characteristics around $\Delta\varphi = 0$.

is $k_{14} = 4.1 \times 10^{-8}$ cm^3 molecule^{-1} s^{-1}, slower by a factor of 7 than the rate coefficient for electron–ion recombination by reaction (10) with $k_{10} = 2.9 \times 10^{-7}$ cm^3 molecule^{-1} s^{-1} [24]. This is the reason why the saturation current i_+(N) at $\Delta\varphi = -50$ V is approximately twice as high for curve (a) than for curve (b) in Fig. 8, or in Fig. 9 at $z = 20$ mm downstream. It also explains why the peak current near $z = 0$ in Fig. 8 is higher for curve (a) than for curve (b). The rate of production of H_3O^+ by way of reactions (8) and (9) should be similar for the two cases because the carbon content is the same. But the rate of ion loss is lower in case (a), resulting in a higher steady-state concentration of H_3O^+ at the current peak.

In Fig. 8(b), saturation occurs at negative $\Delta\varphi$ when all of the electrons in the H_3O^+/e^- flame plasma are stopped by the electric field in the ion sheath at the nozzle. It is reasonable to suppose that a negative potential gradient builds up in the bulk flame plasma sufficient to hold the electrons stationary throughout the flame. But in Fig. 8(a), saturation requires that not only the electrons but also the much more massive Cl^- negative ions are stopped by the ion sheath, requiring a potential gradient $v_f/\mu_- = 3.4 \times 10^4$ V m^{-1}. In fact, this is easily accomplished because the ion sheath is thin. Its thickness is of the order of the debye length for the plasma, $\lambda_D = (\varepsilon_0 kT_e/e^2 n_e)^{1/2} = 0.11$ mm with $T_e = 2400$ K and n_e(N) $= 0.98 \times 10^{15}$ m^{-3} [29]; here, ε_0 is the permittivity of free space. For the thermalized flame plasma, the ion, electron and neutral gas temperatures are all equal to the flame temperature of 2400 K. For a sheath thickness of $\sim 2\lambda_D = 0.22$ mm, only 7.3 V across the ion sheath are required to provide the potential gradient necessary to stop the flow of Cl^- ions. The inset of Fig. (8) shows that more applied voltage is required to saturate curve (a) with chlorine than curve (b) without chlorine at negative $\Delta\varphi$. The reason is provided by Eq. (6). With chlorine present, the electron concentration is reduced due to negative ion formation; thus, more applied voltage is required to reduce $\Delta\varphi_g$ sufficiently so that the saturation electron current is able to flow across the burner gap.

The saturation current at positive $\Delta\varphi$ in Fig. 8 which yields a value of n_+(B) is slightly smaller for

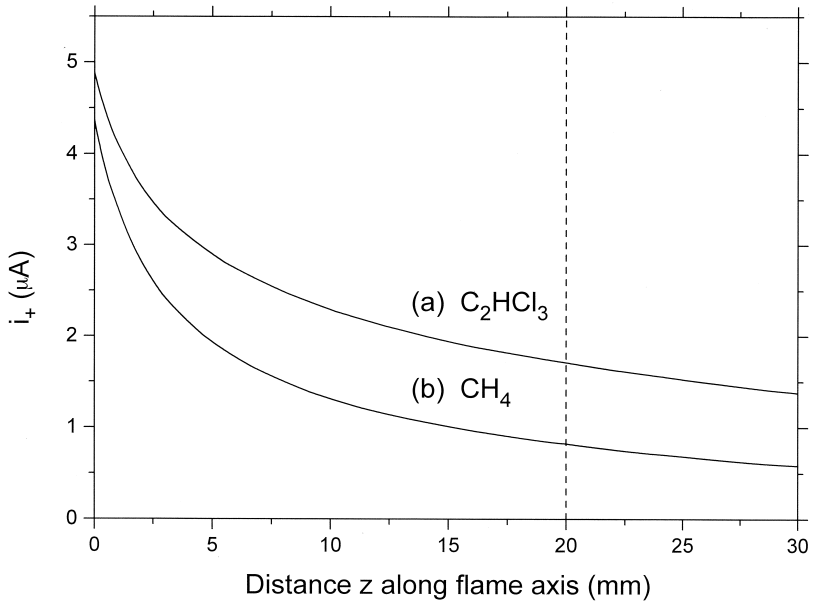

Fig. 9. Current profiles along the flame axis z at $\Delta\varphi = -50$ V for the same flame plasmas involving (a) $H_3O^+/Cl^-/e^-$ and (b) H_3O^+/e^- as those presented in Fig. 8.

curve (a) with chlorine than for curve (b) without. Since n_+(B) has been interpreted above as the total ion production in the reaction zone and since the carbon content in the flames for case (a) and case (b) is the same, i_+(B) for the two cases should also be the same. The decrease observed for i_+(B) in case (a) of Fig. 8 would occur if the radical concentrations, e.g. of CH and O, in the flame reaction zone were reduced by reaction with Cl and HCl, thereby lowering the ion production rate by reaction (8). This is the operative mechanism for flame inhibition in old-fashioned halogen fire extinguishers (e.g. putting CCl_4 on a fire!). The higher peak value at $z = 0$ in Fig. 9(a) is not inconsistent. As discussed previously, the saturation values at $\Delta\varphi > 0$ in Fig. 8 represent total ion production whereas the peak values for $z = 0$ at $\Delta\varphi < 0$ represent a balance of ion production and ion loss. Apparently the lower loss rate due to slower ion-ion recombination raises the peak value in Fig. 9(a) above that in Fig. 9(b).

In summary, the effects of negative ions on the overall i–V characteristic, even when the ratio of $[Cl^-]/[e^-]$ is large, amount to relatively small perturbations of the corresponding characteristic with negative ions absent. However, that statement requires closer scrutiny when $\Delta\varphi$ is close to zero where diffusion effects may be significant. This is the condition which has been employed in the past when sampling positive and negative ions through a nozzle into a mass spectrometer. It will be discussed in detail in a future article on mass-spectrometric sampling.

One final consideration concerning the detailed geometry of the flame and the electrodes (nozzle N and burner B) applies to the whole study. The actual nozzle protrudes slightly from the electrode N distorting its truly planar geometry, and the flame gas aerodynamically diverges when it strikes N distorting its cylindrical shape; both are evident in Fig. 1. The concern is the effect these distortions might have on the shapes of the experimental i–V characteristics and profiles. However, it has already been explained that i_e(N) and i_-(N) when $\Delta\varphi$ is positive are controlled by the flow of positive ions to the burner B, but B has truly planar geometry. Current flow to B also controls the shape in the retardation region when $\Delta\varphi$ goes negative from zero, e.g. Figs. 3, 5, and 8. Conceivably a little distortion might occur around the knee of these characteristics near $\Delta\varphi \sim -5$ V, but the effect on the

saturation current would be minimal. Perhaps the worst case for distortion might be expected for profiles at small values of z measured with $\Delta\varphi = -50$ V because i_+(N) is controlled by the convective flow of positive ions to N. However, distortion is not evident in Figs. 4(a), 6(a), and 9; in any case, the upstream portion of these profiles is not employed for any quantitative purpose. Also, no differences in shape were noted when N was replaced by an uncooled flat plate or a mesh electrode, both of stainless steel. Thus, it is concluded that departures of the flame from cylindrical geometry, or of the nozzle electrode N from planar geometry, do not have a noticeable influence on the quantitative results reported. The major findings, applications and conclusions of the present paper are summarized in the abstract.

Acknowledgements

Support of this work by the Natural Sciences and Engineering Research Council (NSERC) of Canada is gratefully acknowledged. The authors wish to thank Professor J.G. Laframboise of the Department of Physics and Astronomy, York University for helpful discussions. One of the authors (J.M.G.) is grateful to Churchill College, University of Cambridge for the award of a By-Fellowship covering a period of this research in Cambridge, England.

References

[1] A.N. Hayhurst, D.B. Kittelson, N.R. Telford, Combust. Flame 28 (1977) 137.
[2] A.N. Hayhurst, N.R. Telford, Proc. R. Soc. London, Ser. A 322 (1971) 483.
[3] J.M. Goodings, N.S. Karellas, Int. J. Mass Spectrom. Ion Processes 62 (1984) 199.
[4] S.D.T. Axford, A.N. Hayhurst, Bull. Soc. Chim. Belg. 99 (1990) 451.
[5] S.D.T. Axford, A.N. Hayhurst, Twenty-third Symposium (International) on Combustion, The Combustion Institute, Pittsburgh, 1990, p. 363.
[6] S.D.T. Axford, A.N. Hayhurst, Int. J. Mass Spectrom. Ion Processes 110 (1991) 31.
[7] S.D.T. Axford, J.M. Goodings, A.N. Hayhurst, Combust. Flame 114 (1998) 294.
[8] R.M. Clements, P.R. Smy, J. Phys. D: Appl. Phys. 26 (1993) 1916.
[9] J. Dawe, S.A.H. Rizvi, P.R. Smy, IEEE Trans. Plasma Sci. 21 (1993) 202.
[10] C.S. MacLatchy, H.C.L. Smith, IEEE Trans. Plasma Sci. 19 (1991) 1254.
[11] C.H. Su, S.H. Lam, Phys. Fluids 6 (1963) 1479.
[12] S.H. Lam, AIAA J. 2 (1964) 256.
[13] J.M. Goodings, C.S. Hassanali, P.M. Patterson, C. Chow, Int. J. Mass Spectrom. Ion Processes 132 (1994) 83.
[14] J.M. Goodings, S.M. Graham, W.J. Megaw, J. Aerosol Sci. 14 (1983) 679.
[15] J.M. Goodings, C.S. Hassanali, Int. J. Mass Spectrom. Ion Processes 101 (1990) 337.
[16] L.S. Frost, J. Appl. Phys. 32 (1961) 2029.
[17] D. Bradley, S.M.A. Ibrahim, Combust. Flame 22 (1974) 43.
[18] J.B. Hasted, Physics of Atomic Collisions, Butterworths, London, 1964, pp. 18–23.
[19] F.F. Chen, in Plasma Diagnostic Techniques, R.H. Huddlestone, S.L. Leonard (Eds.), Academic, New York, 1965, p. 113.
[20] A.F. Ashton, A.N. Hayhurst, Combust. Flame 21 (1973) 69.
[21] M.I. Boulos, P. Fauchais, E. Pfender, Thermal Plasmas, Fundamentals and Applications, Vol. 1, Plenum, New York, 1994, p. 178.
[22] H.F. Calcote, Eighth Symposium (International) on Combustion, Williams & Wilkins, Pittsburgh, PA, 1962, p. 184.
[23] J.A. Green, T.M. Sugden, Ninth Symposium (International) on Combustion, Academic, New York, 1963, p. 607.
[24] C.J. Butler, A.N. Hayhurst, J. Chem. Soc., Faraday Trans. 92 (1996) 707.
[25] A.G. Gaydon, H.G. Wolfhard, Flames, 4th ed., Oxford University Press, New York, 1979.
[26] N.A. Burdett, A.N. Hayhurst, Proc. R. Soc. London, Ser. A 355 (1977) 377.
[27] M.W. Chase Jr., C.A. Davies, J.R. Downey Jr., D.J. Frurip, R.A. McDonald, A.N. Syverud, JANAF Thermochemical Tables, 3rd ed., J. Phys. Chem. Ref. Data 14 (1985) (Suppl. 1).
[28] N.A. Burdett, A.N. Hayhurst, J. Chem. Soc., Faraday Trans. 1 72 (1976) 245.
[29] F.F. Chen, Introduction to Plasma Physics, Plenum, New York, 1974, p. 10.